

RESEARCH ARTICLE

10.1002/2015JD024203

Key Points:

- Aircraft profiling finds large NO_x vertical gradients in the polluted boundary layer (BL)
- The NO_x vertical gradient is sensitive to the boundary layer stability
- A well-mixed BL assumption causes biases in calculating BL ozone production rate and NO₂ retrievals

Supporting Information:

- Figures S1–S4 and Tables S1 and S2

Correspondence to:

Y. Zhang,
yzhang425@gatech.edu

Citation:

Zhang, Y., et al. (2016), Large vertical gradient of reactive nitrogen oxides in the boundary layer: Modeling analysis of DISCOVER-AQ 2011 observations, *J. Geophys. Res. Atmos.*, 121, doi:10.1002/2015JD024203.

Received 8 SEP 2015

Accepted 24 JAN 2016

Accepted article online 27 JAN 2016

Large vertical gradient of reactive nitrogen oxides in the boundary layer: Modeling analysis of DISCOVER-AQ 2011 observations

Yuzhong Zhang¹, Yuhang Wang¹, Gao Chen², Charles Smeltzer¹, James Crawford², Jennifer Olson², James Szykman^{3,2}, Andrew J. Weinheimer⁴, David J. Knapp⁴, Denise D. Montzka⁴, Armin Wisthaler^{5,6}, Tomas Mikoviny^{7,8}, Alan Fried⁹, and Glenn Diskin²

¹School of Earth and Atmospheric Sciences, Georgia Institute of Technology, Atlanta, Georgia, USA, ²NASA Langley Research Center, Hampton, Virginia, USA, ³National Exposure Research Laboratory, US Environmental Protection Agency, Research Triangle Park, North Carolina, USA, ⁴Atmospheric Chemistry Division, National Center for Atmospheric Research, Boulder, Colorado, USA, ⁵Institut für Ionenphysik und Angewandte Physik, Universität Innsbruck, Innsbruck, Austria, ⁶Department of Chemistry, University of Oslo, Oslo, Norway, ⁷Oak Ridge Associated Universities, Oak Ridge, Tennessee, United States, ⁸Now at Department of Chemistry, University of Oslo, Oslo, Norway, ⁹University of Colorado Boulder, Boulder, Colorado, USA

Abstract An often used assumption in air pollution studies is a well-mixed boundary layer (BL), where pollutants are evenly distributed. Because of the difficulty in obtaining vertically resolved measurements, the validity of the assumption has not been thoroughly evaluated. In this study, we use more than 200 vertical profiles observed in the Deriving Information on Surface Conditions from Column and Vertically Resolved Observations Relevant to Air Quality (DISCOVER-AQ) aircraft campaign in July 2011 to examine the vertical distributions of pollutants over the Washington-Baltimore area. While many long-lived species are well mixed in daytime, the observed average vertical profile of NO_x shows a large negative gradient with increasing altitude in the BL. Our analysis suggests that the magnitude of the NO_x gradient is highly sensitive to atmospheric stability. We investigate how parameterizations of the BL and land-surface processes impact vertical profiles in a 1-D chemical transport model, using three BL schemes (Asymmetric Convective Model version 2 (ACM2), Yonsei University (YSU), and Mellor-Yamada-Janjic (MYJ)) and two land-surface schemes (Noah and Rapid Update Cycle (RUC)). The model reasonably reproduces the median vertical profiles of NO_x under different BL stability conditions within 30% of observations, classified based on potential temperature gradient and BL height. Comparisons with NO_x observations for individual vertical profiles reveal that while YSU performs better in the turbulent and deep BL case, in general, ACM2 (RMSE = 2.0 ppbv) outperforms YSU (RMSE = 2.5 ppbv) and MYJ (RMSE = 2.2 ppbv). Results also indicate that the land-surface schemes in the Weather Research and Forecasting (WRF) model have a small impact on the NO_x gradient. Using model simulations, we analyze the impact of BL NO_x gradient on the calculation of the ozone production rate and satellite NO₂ retrieval. We show that using surface measurements and the well-mixed BL assumption causes a ~45% high bias in the estimated BL ozone production rate and that the variability of NO₂ vertical profiles is responsible for 5–10% variability in the retrieved NO₂ tropospheric vertical columns.

1. Introduction

The lowest part of atmosphere is directly influenced by diurnal heat, moisture, or momentum transfer to or from the surface and thus is referred to as the boundary layer (BL). The vertical distribution of air pollutants in the boundary layer is a complex function of emissions, advection, chemistry, and turbulent mixing. Based on the reasoning that vigorous turbulent mixing in the BL is much faster than chemical loss for many species of interest, air pollution studies often assume a well-mixed BL, where pollutants are evenly distributed. This assumption enables researchers to infer average conditions in the BL from surface observations [e.g., Petritoli *et al.*, 2004; Fiedler *et al.*, 2005; Leigh *et al.*, 2007; Lee-Taylor *et al.*, 2011; de Arellano *et al.*, 2011; Knepp *et al.*, 2013] and thus greatly extends the use of surface measurements. This assumption readily works as a first-order approximation for long-lived species such as carbon monoxide and ethane but is invalid for very reactive species such as isoprene. However, for moderately reactive species which has a chemical lifetime comparable to the BL mixing time scale, the validity of the well-mixed BL assumption over emission regions and its implications have not been evaluated.

One such species is nitrogen oxides (NO_x = NO₂ + NO), a primary pollutant that plays a critical role in the formation of tropospheric ozone [e.g., Liu *et al.*, 1992; Chameides *et al.*, 1992], nitrate aerosol [e.g., Bassett and

Seinfeld, 1983], and secondary organic aerosol [e.g., Ng *et al.*, 2007]. Previous studies find quite substantial differences in vertical profiles of NO_x among 3-D model simulations [Huijnen *et al.*, 2010; Russell *et al.*, 2011; Boersma *et al.*, 2011]. Loss of NO_x through formation of nitric acid and organic nitrates results in a NO_x chemical lifetime of several hours in daytime during the summer, which is comparable to the BL mixing time scale, indicating that the vertical distribution of NO_x may be sensitive to the relative importance between chemical loss and turbulent mixing. Inadequate knowledge of the vertical distributions of NO_x can lead to biases in a variety of calculations, for example, the calculation of the BL-averaged ozone production rate [Liu *et al.*, 2012a] and satellite NO_2 retrieval [Boersma *et al.*, 2004; Gu *et al.*, 2014].

In this work, we will use aircraft measurements from the NASA Earth Venture campaign in July 2011, Deriving Information on Surface Conditions from Column and Vertically Resolved Observations Relevant to Air Quality (DISCOVER-AQ 2011), to investigate the factors regulating the vertical profile of NO_x . Previous aircraft campaigns (e.g., INTEX-A, INTEX-NA, and NEAQS) have reported a large gradient of NO_x between the BL and free troposphere over the polluted continent [Martin *et al.*, 2006; Singh *et al.*, 2007; Boussez *et al.*, 2007; Zhao *et al.*, 2009a; Boersma *et al.*, 2011]. However, because these aircraft campaigns aimed at sampling the whole troposphere over vast regions, the data from these campaigns cannot be used to resolve the vertical distribution of NO_x within the BL. DISCOVER-AQ is unique in that the BL and lower free troposphere were systematically sampled to obtain a large data set of vertical profiles of trace gases and aerosols and that the horizontal gradient confounding the interpretation of aircraft measurements was also reduced by spiral profiling.

The remainder of the paper proceeds as follows. Section 2.1 describes the observational data collected during DISCOVER-AQ 2011. To gain insight into how BL conditions impact the vertical profile of NO_x , we classify the observed vertical profiles based on BL height and potential temperature gradient in section 2.2. Section 2.3 describes the setup of the 1-D Regional chemical transport Model (1-D REAM). Sections 2.4 and 2.5 describe the calculation of model diagnostics and NO_2 air mass factor, respectively. In section 3.1, we present modeling results and comparisons with observations, based on the profile classification presented in section 2.2. We then explore the sensitivity of the NO_x vertical profile to BL stability in section 3.2. To characterize the uncertainty in the modeling analysis, we analyze in section 3.3 the impact of BL and land-surface parameterizations on the vertical profiles of NO_x . In sections 3.4 and 3.5, we quantitatively assess the influence of the BL NO_x gradient on the calculation of the BL-averaged ozone production rate and tropospheric NO_2 column retrieval, respectively. Finally, in section 4, we summarize our findings.

2. Data and Model

2.1. DISCOVER-AQ Data

During DISCOVER-AQ 2011, 14 research flights using the NASA P-3B aircraft took place around the Washington-Baltimore region (see the online data archive <http://www-air.larc.nasa.gov/missions/discover-aq/discover-aq.html> for the detailed description of the research flights). By performing spiral profiling over six surface sites and occasionally over the Chesapeake Bay (Figure S1 in the supporting information), extensive measurements were made in the BL and the lower free troposphere, providing a total of 253 daytime vertical profiles of various species from ~300 m to 5 km. To calculate these vertical profiles, raw measurements of each spiral flight are binned and averaged based on the model vertical levels in part to remove the fine-scale horizontal variation that cannot be simulated in a 1-D model.

NO , NO_2 , and ozone were measured by the National Center for Atmospheric Research 4-channel chemiluminescence instrument [Brent *et al.*, 2013]. Formaldehyde was measured by a difference frequency generation absorption spectrometer [Weibring *et al.*, 2010]. Volatile organic compounds, including isoprene, toluene, and xylene, were measured using a proton-transfer-reaction mass spectrometer [Lindinger *et al.*, 1998]. CO was measured by a diode laser spectrometer [Sachse *et al.*, 1987]. The uncertainties of the measurements are about 10% for NO , 15% for NO_2 , 5% for ozone, 4% for formaldehyde, 2% or 2 ppbv for CO , and 10% for volatile organic compounds, respectively (Table S1).

2.2. Classification of Vertical Profiles

To investigate the impact of turbulent mixing on the vertical profile of NO_x , we classify over 200 vertical profiles based on BL height and stability. The BL height is determined as the height where the potential temperature gradient is larger than 5 K/km [Heffter, 1980]. We classify a vertical profile as “deep,” “medium,” or “shallow” if

the BL height is higher than 1 km, between 0.5 km and 1 km, or lower than 0.5 km, respectively. To characterize the stability of the BL, we calculate the average linear potential temperature gradient within the BL ($\partial\theta/\partial z$). We classify a vertical profile as “turbulent,” “neutral,” or “stable” if $\partial\theta/\partial z$ in the BL is less than 0.1 K/km, between 0.1 K/km and 1 K/km, or greater than 1 K/km, respectively. Note that our definitions of turbulent, neutral, or stable BL are different from conventional ones, in which unstable, neutral, or stable BL is usually defined as $\partial\theta/\partial z$ less than, equal to, or greater than 0 K/km, respectively. Our definition is designed based on the DISCOVER-AQ 2011 data to reflect the nonlinear scale observed in the relationship between the BL NO_x vertical gradient and BL stability during the campaign (see discussions in section 3.2). It is also noteworthy that DISCOVER-AQ 2011 conducted in the daytime of summer represents a relatively turbulent BL. The stable case referred here is relative to the other less stable cases during the campaign. The largest $\partial\theta/\partial z$ in the BL observed during the campaign is ~ 1.6 K/km. It is not uncommon to observe a greater BL $\partial\theta/\partial z$, for example, in a temperature inversion BL. It will be interesting if future analysis can include more data to resolve a complete spectrum of boundary layer stability.

Table 1 shows a summary of profile classification. Because our algorithm cannot identify the BL height for some of the vertical profiles, the total count of classified profiles is 209. The vertical profiles in DISCOVER-AQ 2011 distribute unevenly among the categories. The dominant category is “deep and neutral” (123 profiles), accounting for more than half of all classified vertical profiles. Following deep and neutral are categories “deep and turbulent” (40 profiles), “medium and neutral” (24 profiles), “shallow and stable” (12 profiles), and “medium and stable” (7 profiles). As expected, the two dimensions, BL height and BL stability, overlap to a large extent, and no profile falls in the categories “deep and stable,” “medium and turbulent,” “shallow and turbulent,” and “shallow and neutral.” Therefore, we exclude these four categories in our discussion. Because shallow and stable and medium and stable categories show similar vertical profiles and the profile numbers are relatively low, we also merge these two groups into the category stable so as to simplify our discussion.

Table 2 summarizes the distribution of profile categories among the time of the day and among surface sites. As a result of the sampling design, the classified vertical profiles are more frequent toward midday (10:00–14:00 LT) than late afternoon (14:00–18:00 LT) and early morning (6:00–10:00 LT). On the other hand, the distributions of classified vertical profiles are similar among various sites, except for Chesapeake Bay and Beltsville. The underrepresentation of the Beltsville site is partly due to air traffic control, which leads to difficulty in identifying the BL height from inadequate vertical sampling. Because of the cooler water surface relative to land at daytime, the BL over the Chesapeake Bay tends to be more shallow and stable. The similar category distributions of vertical profiles among land sites reflect homogeneity of BL conditions over the region. Table 2 also shows that deep and turbulent and deep and neutral cases are more frequent, and stable cases are less frequent in midday and late afternoon than in early morning. However, it is noteworthy that we also find a few deep and turbulent and deep and neutral cases in the morning and a few stable cases in the afternoon. We also summarize in Table S2 in the supporting information the distribution of profile categories with respect to the flights, which depends on the day-to-day variation of BL mixing as well as the aircraft sampling design (e.g., time of the day).

2.3. 1-D REAM Model

In this work, we will use the one-dimensional version of the Regional chEmical trAnsport Model (1-D REAM) to analyze the vertical profile of NO_x during DISCOVER-AQ 2011. The 1-D REAM has been applied in studies on urban photochemistry in China [Liu *et al.*, 2010, 2012a, 2014], polar photochemistry at the South Pole [Wang *et al.*, 2007], and marine chemistry over the tropical Pacific [Gray *et al.*, 2011; Zhang *et al.*, 2014]. The 1-D REAM is a column chemical transport model that has 30 vertical layers in the troposphere, with 15 layers below 2000 m (centered at $\sim 15, 40, 70, 120, 170, 210, 290, 370, 500, 650, 850, 1050, 1250, 1450, \text{ and } 1700$ m). The 1-D REAM inherits relevant modules for photochemistry, convective transport, vertical diffusion, and wet/dry deposition from the original 3-D REAM [Choi *et al.*, 2005, 2008a, 2008b; Zhao and Wang, 2009; Zhao *et al.*, 2009a, 2009b; Yang *et al.*, 2010; Zhao *et al.*, 2010; Liu *et al.*, 2012b; Gu *et al.*, 2013, 2014]. Chemical kinetics data are updated following the latest compilation by Sander *et al.* [2011], with expansion on volatile organic compound (VOC) chemistry [Liu *et al.*, 2010]. Meteorological parameters (e.g., water vapor concentrations, temperature, pressure, and the diffusion coefficient) are obtained from WRF-assimilated meteorological fields constrained by the Climate Forecast System Reanalysis data. Photolysis rates are dependent on cloud fraction and optical depth calculated based on WRF meteorological fields [Choi *et al.*, 2008a]. To achieve a quasi steady state, we run the 1-D REAM with a 1 min time step for 20 simulation days with

Table 1. Counts of Vertical Profile Categories, Classified Based On BL Height and Potential Temperature Gradient^a

Stability	Height	Deep>1 km	Medium0.5–1 km	Shallow<0.5 km
Turbulent	<0.1 K/km	40	-	-
Neutral	0.1–1 K/km	123	24	-
Stable	>1 K/km	-	7	12

^aThe predominant category in DISCOVER-AQ 2011 is deep and neutral, which shows a strong sensitivity of the NO_x gradient to BL stability.

repeated diurnal meteorological fields in the day of the observation. Only the results from the last day are used for analysis.

The 1-D REAM is constrained with measurements from DISCOVER-AQ 2011. We specify surface-emitted species, including NO, NO₂, aromatics, and isoprene, with observations at the lowest altitude of aircraft measurements (~300 m). For the practical purpose of 1-D modeling, these values are also assigned to model layers below that because of a lack of reliable observations below ~300 m. However, all analysis results presented in this work are above 300 m. Since a 1-D column model does not simulate advection, which can be significant for the species with relatively long lifetimes such as O₃ and CO, we constrain the model with the measured O₃ and CO (Figure S2f in the supporting information) vertical profiles. The diurnal variations of constrained species (e.g., NO_x at 300 m, O₃) are estimated by aggregating daytime observations when possible. Any measurement data gap is interpolated using 3-D REAM simulation results (e.g., at night). The unmeasured VOCs (e.g., alkanes) are specified at ~300 m with 3-D REAM simulation results. Their effects on O₃ chemistry are not large. For the initial conditions, we use monthly mean vertical profiles generated from 3-D REAM simulation. All model evaluations are done for the time of the observations. Comparing 1-D REAM results with observations, we find that the model is able to reproduce the vertical profile of observed NO_x (Figure 1) and other species (Figures S2a–S2e in the supporting information).

To investigate how the parameterizations of the BL and land-surface processes impact the simulation, we test three BL schemes, Asymmetric Convective Model version 2 (ACM2) [Pleim, 2007], Yonsei University (YSU) [Hong et al., 2006], and Mellor-Yamada-Janjic (MYJ) [Mellor and Yamada, 1982; Janjić, 1990] and two land-surface schemes, Noah and RUC, in the WRF model. For MYJ and YSU, we use a local turbulent diffusion scheme to do the vertical mixing. Although YSU includes nonlocal terms in its formulation, the local turbulent diffusion scheme is used because of the lack of a consistent treatment for meteorological parameters and chemical tracers [Pleim, 2011]. For the hybrid local and nonlocal scheme ACM2, we implement the vertical transport scheme following Pleim [2007]. For comparison purposes, the sensitivity tests of BL schemes use only the Noah land-surface scheme and the sensitivity tests of land-surface schemes use only the MYJ BL scheme. Section 3.3 summarizes and compares the performance of these BL and land-surface schemes.

2.4. Model Diagnostics

To investigate the factors controlling the vertical profile, we compute chemical lifetime (τ_c) and turbulent mixing time (τ_m) using model results. τ_c varies from species to species and is calculated as $\tau_c = [X]/L_x$, where

Table 2. Distributions of Profile Categories With Respect to Local Time and Location During DISCOVER-AQ 2011

	Deep and Turbulent	Deep and Neutral	Medium and Neutral	Stable	Total
<i>Distribution of Profile Categories at Varied Local Time</i>					
6:00–10:00	2	10	8	9	29
10:00–14:00	29	75	12	7	123
14:00–18:00	9	38	4	3	54
<i>Distribution of Profile Categories at Varied Sites</i>					
Padonia	5	24	2	3	34
Fairhill	9	25	5	1	40
Aldino	8	21	5	2	36
Edgewood	7	27	5	2	41
Essex	6	22	3	3	34
Beltsville	5	3	3	4	15
Chesapeake Bay	0	1	1	4	6

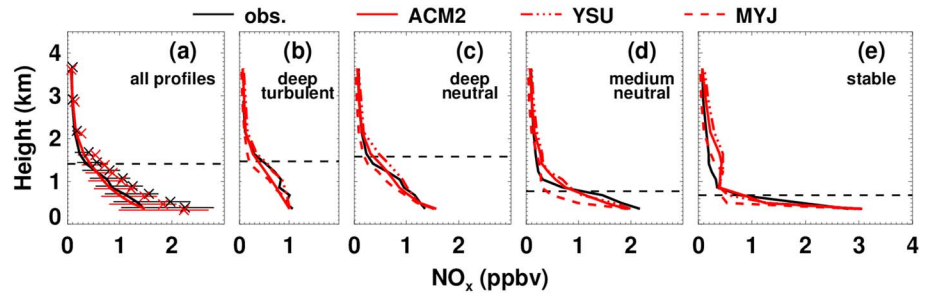


Figure 1. (a) Observed (black) and simulated (red) median vertical profiles of NO_x during DISCOVER-AQ 2011. Error bars indicate the interquartile ranges, and crosses show the arithmetic means. (b–e) Observed (black) and modeled (red) median vertical profile of NO_x for varied profile categories: (Figure 1b) deep and turbulent, (Figure 1c) deep and neutral, (Figure 1d) medium and neutral, and (Figure 1e) stable. Red lines show simulated results using ACM2 (solid), YSU (dash dotted), and MYJ (dashed). Horizontal dashed lines show the average boundary layer height for each category.

[X] is modeled concentration of species X and L_x the chemical loss rate of X. For example, L_{NO_x} includes NO_x loss to nitric acid (HNO_3), peroxyacetyl nitrate, and other organic nitrates. The uncertainty of the τ_c estimate reflects the uncertainties of kinetics rate constants and model estimated reactants such as OH and peroxyacetyl radicals. On the other side, τ_m is independent of the species in question and is defined as the time that a model layer takes to accumulate the concentration of an inert gas to 1/e of the first layer, given a fixed concentration in the first layer and zero initial concentrations in the rest of model layers. We use a simplified 1-D model with only vertical turbulent transport driven by the WRF-generated vertical turbulent diffusivity to calculate τ_m .

Using the simulated concentrations of NO, HO_2 , and various peroxy radicals (RO_2), we diagnose the vertical profile of the ozone production rate and derive the BL-averaged ozone production rate. The ozone production rate, $P(\text{O}_3)_i$, is calculate as

$$P(\text{O}_3)_i = k_{0,i}[\text{NO}]_i[\text{HO}_2]_i + \sum_{j=1}^n k_{j,i}[\text{NO}]_i[\text{RO}_2]_{j,i},$$

where i denotes the model layer, j denotes the numbering of RO_2 , $k_{0,i}$ is the rate constant for the $\text{NO} + \text{HO}_2$ reaction, $k_{j,i}$ is the rate constant for a specific $\text{NO} + \text{RO}_2$ reaction, and $[\text{NO}]_i$, $[\text{HO}_2]_i$, and $[\text{RO}_2]_{j,i}$ are concentrations for NO, HO_2 , and various RO_2 radicals. RO_2 includes CH_3O_2 and other organic proxy radicals derived from oxidation of alkanes, alkenes, aromatics, and isoprene. The BL-averaged ozone production rate, denoted as $P(\text{O}_3)_{\text{BL}}$, is calculated as the average of the ozone production rate in each layer within the BL weighted with the layer thickness

$$P(\text{O}_3)_{\text{BL}} = \frac{\sum_{i=k_{\text{BLB}}}^{k_{\text{BLT}}} P(\text{O}_3)_i \cdot h_i}{h_{\text{BL}}},$$

where h_i is the thickness of layer i , k_{BLB} is the lowest model layer with aircraft observations (i.e., ~300 m), k_{BLT} is the model layer that encloses the BL top, and h_{BL} is the thickness between the BL top and the lowest model layer with aircraft observations. We also compute the vertical profile of the net ozone production rate ($N(\text{O}_3) = P(\text{O}_3) - L(\text{O}_3)$) and the BL-averaged net ozone formation rate

$$N(\text{O}_3)_{\text{BL}} = \frac{\sum_{i=k_{\text{BLB}}}^{k_{\text{BLT}}} N(\text{O}_3)_i \cdot h_i}{h_{\text{BL}}}.$$

2.5. Calculation of the NO_2 Air Mass Factor

The air mass factor (AMF), defined as the ratio of the slant column (photon path from the sun to the satellite) observed by a satellite to the vertical column to be retrieved, is a key quantity in retrieving the NO_2 tropospheric column [Boersma et al., 2011]. In addition to satellite measurement error, the AMF calculation constitutes an important source of retrieval error [Boersma et al., 2004]. Studies have shown that uncertainties in NO_2 a priori profile shape lead to biases in the AMF [Boersma et al., 2004, 2011].

The AMF is calculated as an average of altitude-dependent AMFs weighted by a prescribed NO₂ vertical profile, following the equation

$$\text{AMF} = \frac{\int \text{amf}_h \cdot c_h \cdot dh}{\int c_h \cdot dh},$$

where amf_h is the altitude-dependent AMF that describes the sensitivity to NO₂ at altitude h and c_h is the prescribed concentration of NO₂ at altitude h and is usually provided by a 3-D chemical transport model. Our calculation includes the whole simulated tropospheric column. As mentioned in section 2.3, we assign a well-mixed lowest 300 m in the 1-D simulation. We will briefly discuss in section 3.5 how the gradient in the lowest 300 m affect the AMF calculation. In addition, because the upper troposphere is not sampled in the DISCOVER-AQ 2011 data, the calculation does not include information about the tropospheric lightning NO_x; thus, it is a low-end estimate of the AMF. The altitude-dependent AMF, amf_h , is calculated with the Doubling Adding KNMI (DAK) version 2 model [Boersma *et al.*, 2011]. The WRF meteorological parameters are used for the DAK model. Surface albedo is assigned as 0.05. For the simplicity of comparison, we also assume a nadir view of the hypothetical satellite and the solar zenith and azimuth angle to be 22° and 0°, respectively.

Based on simulated NO₂ vertical profiles, we calculate the AMF for each individual profiles (AMF_{ind}) and the AMF for site-average and campaign average vertical profiles (AMF_{avg}). The difference between AMF_{ind} and AMF_{avg} provides information on how the temporal variation in vertical profiles impacts NO₂ column retrievals. To explore the contribution of BL stability to the temporal variability, we calculate the AMF for each profile category.

3. Results and Discussion

3.1. NO_x Vertical Profiles

Figure 1a shows good agreement (within 20%) between the observed and simulated median vertical profiles of NO_x. Table 3 summarizes the statistics of model-observation comparison for each vertical profile category using varied BL and land-surface schemes. Since the aircraft sampling during DISCOVER-AQ 2011 was usually conducted in daytime with no significant cloud cover reported, a well-developed BL is expected. In fact, the average BL height during aircraft sampling is 1.4 km (standard deviation 0.5 km). However, to the contrary of what a well-mixed BL would suggest, both the observations and model simulations show a substantial vertical gradient of NO_x. The median concentration of NO_x decreases from 1.5 ppbv at ~300 m to 0.4 ppbv at the average BL height during the campaign (1.4 km), a 70% concentration decrease in 1.1 km. A closer examination of individual NO_x vertical profile affirms the prevailing negative gradient of NO_x in the BL during the campaign. The magnitude of the gradient, however, varies greatly from profile to profile (Figure 2a).

Although not dedicated to the vertical gradient of NO_x in the BL, a few previous studies trying to link column tropospheric NO₂ to surface concentration hinted at the effects of the vertical gradient [Petritoli *et al.*, 2004; Knepp *et al.*, 2013]. Assuming a well-mixed BL, these studies derived surface NO₂ (C_{derived}) from dividing column NO₂ measurements by BL height and compared C_{derived} to surface measurements (C_{measured}). Regression analysis ($C_{\text{derived}} = a \cdot C_{\text{measured}} + b$) showed that the slope, a , is always less than one, indicating that column-derived surface NO₂ tends to underestimate particularly in the summer when NO_x is assumed to be well mixed in the BL.

3.2. Sensitivity of NO_x Gradient to BL Stability

Figure 2a shows that the relationship between the BL NO_x gradient and BL stability (i.e., potential temperature (θ) gradient) has roughly three regimes. When the BL is in the turbulent regime ($\partial\theta/\partial z < 0.1$ K/km), NO_x is well mixed; when the BL is in the stable regime ($\partial\theta/\partial z > 1$ K/km), the magnitude of the NO_x gradient in the BL is largest (median gradient at ~−3 ppbv/km); most interestingly, when the BL is in the transitional regime (0.1 K/km $< \partial\theta/\partial z < 1$ K/km), the vertical gradient of NO_x in the BL appears to be highly sensitive to BL stability (or θ gradient). Based on this observation, we define in section 2.2 the criteria for turbulent, neutral, and stable categories. The predominance of the deep and neutral category (Table 1) implies that even when the BL is well developed, it is common that the atmosphere is in the neutral or transitional regime, in which the vertical gradient of NO_x is sensitive to BL stability.

Table 3. Performance of BL and Land-Surface Schemes for Different Profile Categories^a

	Deep and Turbulent			Deep and Neutral			Medium and Neutral			Stable		
	Bias	R	RMSE	Bias	R	RMSE	Bias	R	RMSE	Bias	R	RMSE
<i>BL Schemes</i>												
MYJ	-0.23	0.66	0.94	0.01	0.46	2.17	-0.10	0.73	0.92	-0.14	0.77	1.18
YSU	-0.07	0.83	0.67	0.32	0.44	2.49	0.24	0.71	1.07	0.09	0.87	0.90
ACM2	-0.20	0.82	0.73	0.13	0.50	2.06	0.14	0.75	0.90	0.04	0.88	0.89
<i>Land-Surface Schemes</i>												
Noah	-0.23	0.66	0.94	0.01	0.46	2.17	-0.10	0.73	0.92	-0.14	0.77	1.18
RUC	-0.26	0.64	0.97	-0.01	0.44	2.20	-0.12	0.72	0.94	-0.18	0.72	1.30

^aMetrics for performance of simulated NO_x mixing ratios include bias, correlation coefficient (R), and root-mean-square error (RMSE). Bias and RMSE are in the unit of parts per billion by volume and R value is unitless.

The vertical gradient over a homogeneous region is largely a result of the competition between chemical loss and turbulent mixing. While chemical loss is determined by the chemical property of the species of interest and the photochemical environment (i.e., abundance of radiation and the other reactants in the loss reactions), turbulent mixing is a function of BL stability. Qualitatively, for a surface-emitted species, fast (slow) chemical loss and slow (fast) vertical mixing contribute to a large (small) vertical gradient. In Figure 2b, we show average chemical lifetime (τ_c) and turbulent mixing time (τ_m) as a function of altitude for all categorized profiles and each profile category. Consistent with previous studies conducted during the summer over the eastern U.S. [Spicer, 1982; Sillman, 2000], τ_c for NO_x during DISCOVER-AQ 2011 is 2–5 h throughout the BL, in deep and neutral and deep and turbulent cases, two dominant categories. In the stable case, τ_c is slightly longer (6–9 h), likely due to cloud cover and hence reduced chemical loss. Our calculation shows that the chemical time scales of NO_x and mixing time scales are on the same order of magnitude in the bulk of the BL, consistent with the observation that the BL NO_x gradient is sensitive to BL stability (Figure 2a). The vertical extent of comparable chemical and mixing time scales is much deeper in turbulent and neutral than stable cases, resulting in the observed different NO_x vertical profiles among the categories during the campaign. The difference is mainly attributable to that in BL stability (τ_m) rather than photochemical lifetime (τ_c).

Figure 2b also contrasts NO_x with other species such as isoprene and carbon monoxide (CO). Average τ_c for isoprene is less than an hour, faster than τ_m in the BL, and thus results in a vertical profile with strong gradient in the BL (Figure S2b in the supporting information). On the other hand, average τ_c for CO is about a week, much longer than τ_m , allowing a relatively well-mixed vertical profile in the BL (Figure S2f in the supporting information). However, for long-lived species such as CO, in most cases, advection is also a nonnegligible factor that

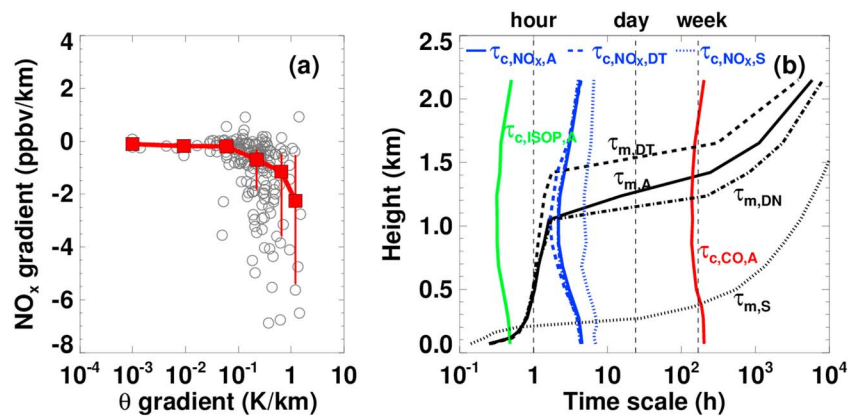


Figure 2. (a) Relationship between the NO_x gradient and the potential temperature (θ) gradient in the BL. Circles represent individual profiles, and red squares represent the medians of NO_x gradients in θ gradient bins. The six bins are defined as 0–0.002, 0.002–0.02, 0.02–0.1, 0.1–0.5, 0.5–1, and 1–10 K/km, respectively. (b) NO_x chemical lifetime (τ_{c,NO_x}) and vertical mixing time scale (τ_m) as a function of height in different cases: deep and turbulent (DT), deep and neutral (DN), stable (S), and all DISCOVER-AQ 2011 profiles (A). Note that NO_x chemical lifetime in the deep and neutral case is not discernible from that for the all profiles and thus is not plotted. To compare, chemical lifetimes of CO ($\tau_{c,CO}$) and isoprene ($\tau_{c,ISOP}$) for all profiles are also plotted.

contributes to the shape of vertical profile. For this reason, vertical profiles of CO are not simulated in the 1-D REAM (see section 2.3).

3.3. Impact of BL and Land-Surface Schemes on NO_x Vertical Profiles

The simulation of vertical profiles depends on model representations of vertical mixing. In the 1-D REAM, vertical mixing is driven by the WRF-generated parameters such as turbulent diffusivity, which is computed by BL and land-surface schemes in WRF. A number of studies compared the performance of these WRF schemes in terms of meteorological parameters such as temperature and humidity [Gilliam and Pleim, 2010; Hu et al., 2010; Shin and Hong, 2011; Xie et al., 2012], but few evaluated their influence on chemical tracers [Yerramilli et al., 2010; Pleim, 2011]. To test how the choices of BL and land-surface schemes impact vertical mixing in the 1-D REAM, we choose three BL schemes (MYJ, YSU, and ACM2) and two land-surface schemes (Noah and RUC) in WRF and evaluate their performance with the DISCOVER-AQ 2011 observations.

Figures 1b–1e show the comparison of simulated median vertical profile using aforementioned BL schemes with observations. The simulated median vertical profiles are within 30% of the observations for varied categories. Statistics for model performance of simulated NO_x mixing ratios for individual vertical profiles, including bias, linear correlation coefficient, and root-mean-squared error (RMSE), are summarized in Table 3. In general, all these schemes are able to generate mixing parameters that result in reasonable agreement with observations. However, the performance of the BL schemes differs among profile categories. For the deep and turbulent category, YSU performs better than MYJ and ACM2 because YSU generates more mixing in the BL than the other two. For deep and neutral and medium and neutral categories, while MYJ produces the least mean bias, ACM2 performs best in terms of correlation and RMSE. Both schemes outperform YSU, which overestimates vertical mixing for the neutral categories. For the stable category, ACM2 performs best among the three schemes.

It is noteworthy that Pleim [2011] points out that the formulation of YSU is inherently inconsistent between meteorological and chemical tracers. As a result, despite YSU being a nonlocal scheme, its implementation in the 1-D REAM only utilizes the vertical diffusion coefficient generated from WRF. This inconsistency may cause more BL mixing with the YSU scheme in our test. On the other hand, although the inclusion of nonlocal terms in ACM2 does enhance vertical mixing relative to the local scheme MYJ, ACM2 still seems to underestimate in turbulent cases. Unlike BL schemes, two land-surface schemes result in negligible difference in performance for all profile categories (Table 3). It is also noteworthy that the 1-D REAM well constrains local NO_x emissions by specifying observed concentrations at ~300 m. For 3-D chemical transport models, however, in addition to the BL and land-surface schemes, other factors such as emissions and model resolutions also contribute to shaping the vertical NO_x profiles [Huijnen et al., 2010].

In summary, we find that while YSU outperforms the other two schemes for the deep and turbulent category, ACM2 has the best overall performance, including the most dominant category, deep and neutral, during DISCOVER-AQ 2011. We also find that two land-surface schemes result in small differences in performance. Based on these results, we recommend the use of the ACM2 BL scheme and the Noah or RUC land-surface scheme in WRF simulations for air pollution modeling.

3.4. BL-Averaged Ozone Production Rate

The net ozone production rate, $P(O_3)$, calculated as the sum of reaction rates of NO with HO₂ and organic RO₂ (see section 2.4 for details), quantifies how fast the in situ chemical production of ozone occurs. The calculation of $P(O_3)$ is required in the diagnosis of the ozone production regime [Liu et al., 2012a]. Many studies report surface $P(O_3)$ based on ground level measurements [e.g., Ren, 2003; Shirley et al., 2006; Kanaya et al., 2008]. However, in principle, because of a relatively long lifetime of ozone, BL-averaged ozone production rate, $P(O_3)_{BL}$, is a more appropriate quantity to characterize the contribution of local chemistry to the surface concentration of ozone. In this regard, the ozone production rate derived from surface measurements, $P(O_3)_{surf}$, can be biased high or low relative to $P(O_3)_{BL}$ if a gradient of $P(O_3)$ exists in the BL. Using the 1-D REAM, Liu et al. [2012a] found that the $P(O_3)_{BL}$ is about a factor of 4 lower than surface $P(O_3)_{surf}$ in highly polluted (high NO_x and high VOC) urban Beijing and the authors attributed it to the large gradient of NO_x in the BL. In this work, with aircraft measurements providing much more information to constrain the model, we derive vertical profiles of $P(O_3)$ and assess the uncertainty of $P(O_3)_{BL}$.

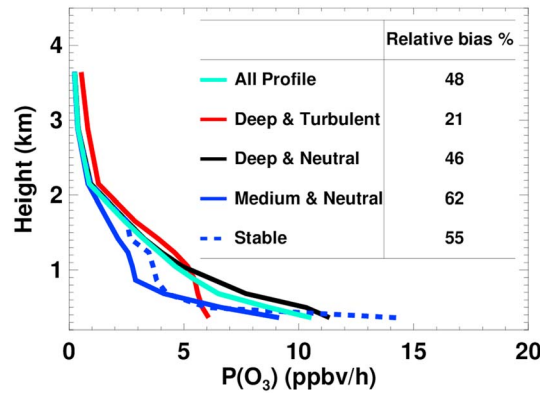


Figure 3. Median vertical profile of $P(O_3)$ for all profiles and each profile category. Relative biases of BL O_3 production rates calculation using an assumed well-mixed NO_x profile in the BL with NO_x measured at ~ 300 m ($P(O_3)_{300\text{ m}}/P(O_3)_{BL} - 1$) are tabulated (inset).

Figure 3 shows that $P(O_3)$ has a substantial gradient within the BL. The campaign median decreases from 10.5 ppbv/h at 300 m to 3 ppbv/h at 1.5 km. $P(O_3)$ of 10 ppbv/h near the surface is comparable to previous studies conducted in U.S. urban regions [e.g., Ren, 2003; Kleinman et al., 2005; Cazorla et al., 2012; Ren et al., 2013]. The analysis also shows that ozone is produced mainly through the reaction of $HO_2 + NO$ ($\sim 80\%$) with minor contribution from organic $RO_2 + NO$ reactions (Figure S3a in the supporting information). In contrast to NO_x , which decreases by 70% in the BL (section 3.1), Figure S3b in the supporting information shows that HO_2 varies slightly from 300 m to 1.5 km ($< 10\%$). Therefore, we conclude that the gradient of $P(O_3)$ in the BL results primarily from the gradient of NO_x rather than that of HO_2 or RO_2 , which is

consistent with Liu et al. [2012a]. In addition, we find that the vertical profiles of the net ozone production rate, $N(O_3)$, are similar to those of $P(O_3)$ because the ozone chemical loss rate during the campaign is relatively small (Figure S4).

To assess the bias induced from approximating $P(O_3)_{BL}$ as $P(O_3)_{surf}$, we calculate the relative difference between the $P(O_3)_{BL}$ and $P(O_3)$ at 300 m. The latter is a proxy for $P(O_3)_{surf}$ because we do not have true surface measurements from aircraft. As shown in Figure 3, $P(O_3)$ at 300 m is on average 48% larger than $P(O_3)_{BL}$, which is close to the value of 46% for the deep and neutral category. The relative bias becomes larger as the BL gets more stable and shallower, from 21% for the deep and turbulent category to 62% for the medium and neutral category. We also find that the relative bias between $N(O_3)_{BL}$ and $N(O_3)$ at 300 m is about 39%, varying from 12% for the deep and turbulent category to 55% for the stable category (Figure S4).

3.5. Tropospheric NO_2 Column Retrievals

Retrievals of tropospheric NO_2 columns from satellite measurements require calculation of the AMF [Boersma et al., 2011]. Estimates in previous studies suggest that the uncertainty in the simulated a priori NO_2 vertical profiles leads to a 5%–15% uncertainty in the calculated AMF [Hains et al., 2010; Boersma et al., 2011; Lin et al., 2014]. Various studies have been devoted to investigate how the uncertainties of NO_2 retrievals are affected

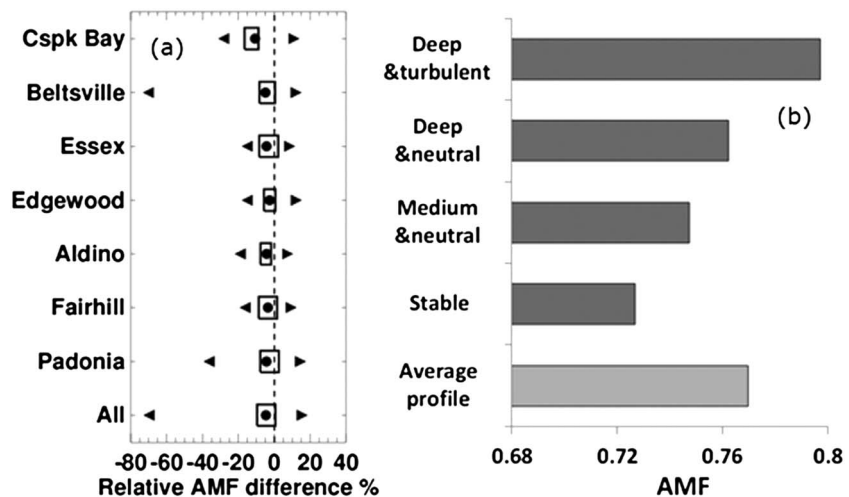


Figure 4. (a) Relative difference between AMF_{ind} and AMF_{avg} ($AMF_{ind}/AMF_{avg} - 1$) at each site and for the whole campaign. Dots represent average, boxes represent interquartile ranges, and triangles represent maximum and minimum of the relative difference, respectively. (b) AMF calculated from average vertical profile for each profile category.

by the a priori NO_2 vertical profile. While a great number of studies [e.g., *Eskes and Boersma, 2003; Boersma et al., 2011; Russell et al., 2011; Heckel et al., 2011*] discuss the impact of the model spatial resolution on NO_2 retrievals, only a few studies have examined the impact of temporal resolution [*Lamsal et al., 2011; Heckel et al., 2011*]. However, different retrieval algorithms sample simulated vertical profiles at varied temporal resolutions, ranging from daily [e.g., *Boersma et al., 2007*], monthly [e.g., *Russell et al., 2011; Valks et al., 2011*], to annually [e.g., *Bucselo et al., 2006*]. In this section, we use the aircraft measurements during DISCOVER-AQ 2011 to assess the impact of variability in NO_2 vertical profiles on the calculation of the AMF.

Figure 4a shows the relative difference of AMF between individual (AMF_{ind}) and average (AMF_{avg}) vertical profiles at various sites. Under the DISCOVER-AQ 2011 conditions, on average, using the campaign average vertical profiles causes $\sim 2\text{--}5\%$ low bias. Additionally, the deviation of individual profiles from the average profile results in about $\pm 5\%$ difference at all sites between AMF_{ind} and AMF_{avg} (the boxes in Figure 4a denote the interquartile relative difference) and even larger difference for particular vertical profiles (the triangles in Figure 4a denote the largest positive or negative relative difference). We suggest that one should take into account this uncertainty in temporal variability along with that in the horizontal resolution when developing and/or evaluating an NO_2 retrieval algorithm.

The statistics shown in Figure 4a are quite consistent across all the sites, indicating that the variability in the AMF can be largely attributed to variability in the mixing property of the BL rather than spatial inhomogeneity. Figure 4b shows that the AMF tends to decrease as the NO_2 gradient becomes sharper in a shallower and more stable BL. The AMFs computed from the average vertical profile for deep and turbulent (0.80), deep and neutral (0.76), medium and neutral (0.75), and stable (0.73) categories are 3.6%, -1.0% , -2.9% , and -5.6% different from that computed from the AMF_{avg} (0.77), respectively. This result shows that the difference in the BL category explains $\sim 5\%$ variability from the AMF_{avg} , supporting the idea that the mixing property of the BL is primarily responsible for the variability of AMF observed in Figure 4a.

In the above calculation of the AMF, we assume a well-mixed profile for the lowest 300 m. To test the sensitivity of the AMF to the near-surface gradient, we also extrapolate the vertical profiles to the surface with the NO_x gradient in the BL and compute the corresponding AMF. The reduction in the AMF resulting from the linear gradient in the lowest 300 m is about 1%, with interquartile range 0.5%–2%. The difference will be more significant if the gradient near the surface is even greater than the bulk BL over the strong source region, as reported previously by some 3-D models [*Huijnen et al., 2010; Boersma et al., 2011*]. Measurements of the lowest few hundred meters in future field experiments will be useful to further reduce the uncertainty of NO_x vertical profile in the AMF calculation.

4. Conclusions

During DISCOVER-AQ 2011, we find frequent occurrences of significant NO_x gradients within the BL, suggesting that the well-mixed BL assumption must be applied cautiously to BL NO_x . The median vertical profile derived from aircraft spirals shows that NO_x concentration decreases by $\sim 70\%$ from 300 m to 1.4 km. The observed vertical profiles of NO_x can generally be reproduced by our 1-D photochemical model driven by WRF-generated meteorological fields. Analysis of the model results shows that the chemical lifetime of NO_x is comparable to the vertical mixing time scale in the BL, resulting in the observed sensitivity of NO_x gradient to BL stability.

Model simulations using different BL and land-surface schemes in WRF found no significant impact on the 1-D model results. All of the three boundary layer schemes (MYJ, YSU, and ACM2) were able to generate a reasonable representation of the vertical mixing under DISCOVER-AQ 2011 conditions. Nonlocal schemes, ACM2 and YSU, moderately improved performance in a turbulent BL, but the YSU scheme tends to overestimate in neutral and stable cases. Using two land-surface schemes (Noah and RUC) resulted in little difference in simulated NO_x vertical profiles.

The gradient of NO_x in the BL can confound the extrapolation of surface measurements to the entire BL. For example, using surface measurements in calculating the ozone production rate in the BL without considering the NO_x gradient can result in a $\sim 45\%$ high bias. In addition, since satellite retrieval of column density utilizes a priori vertical profiles, the model skill to reproduce a realistic vertical profile of NO_x also affects our ability to correctly retrieve tropospheric NO_2 column from satellite measurements. Both spatial and temporal (interday) variations of BL NO_x vertical profiles affect the accuracy of the retrievals.

In this study, we have focused on understanding the vertical profiles of NO_x observed in July 2011 over Washington-Baltimore region during the DISCOVER-AQ campaign. However, we expect that the large gradient of NO_x within the BL is not uncommon. More vertically resolved observations using aircraft, tethered balloon, and remote sensing techniques in other seasons and locations are necessary to understand the implications of BL NO_x gradients on various applications of surface and satellite measurements in air quality studies. In addition, all the results presented here are based on aircraft measurements at least ~ 300 m above ground. Reliable profile measurements in the lowest few hundred meters are also an important area of future field experiments targeting air quality.

Acknowledgments

The data for this paper are available at the DISCOVER-AQ data archive (<http://www-air.larc.nasa.gov/missions/discover-aq/discover-aq.html>). The research was supported by the NASA ACMAP and DISCOVER-AQ programs. We thank David Parrish for his discussion with Y.W. that led to the analyses reported here. PTR-MS measurements of VOCs were supported by the Austrian Federal Ministry for Transport, Innovation, and Technology (BMVIT) through the Austrian Space Applications Programme (ASAP) of the Austrian Research Promotion Agency (FFG). The work of T.M. was supported by an appointment to the NASA Postdoctoral Program at the Langley Research Center administered by Oak Ridge Associated Universities through a contract with NASA.

References

- Bassett, M., and J. H. Seinfeld (1983), Atmospheric equilibrium model of sulfate and nitrate aerosols, *Atmos. Environ.*, *17*(11), 2237–2252, doi:10.1016/0004-6981(83)90221-4.
- Boersma, K. F., H. J. Eskes, and E. J. Brinksma (2004), Error analysis for tropospheric NO_2 retrieval from space, *J. Geophys. Res.*, *109*, D04311, doi:10.1029/2003JD003962.
- Boersma, K. F., et al. (2007), Near-real time retrieval of tropospheric NO_2 from OMI, *Atmos. Chem. Phys.*, *7*(8), 2103–2118, doi:10.5194/acp-7-2103-2007.
- Boersma, K. F., et al. (2011), An improved tropospheric NO_2 column retrieval algorithm for the ozone monitoring instrument, *Atmos. Meas. Tech.*, *4*(9), 1905–1928, doi:10.5194/amt-4-1905-2011.
- Bousserez, N., et al. (2007), Evaluation of the MOCAGE chemistry transport model during the ICARTT/TOP experiment, *J. Geophys. Res.*, *112*, D10S42, doi:10.1029/2006JD007595.
- Brent, L. C., et al. (2013), Evaluation of the use of a commercially available cavity ringdown absorption spectrometer for measuring NO_2 in flight, and observations over the Mid-Atlantic States, during DISCOVER-AQ, *J. Atmos. Chem.*, doi:10.1007/s10874-013-9265-6.
- Bucselo, E. J., E. A. Celarier, M. O. Wenig, J. F. Gleason, J. P. Veefkind, K. F. Boersma, and E. J. Brinksma (2006), Algorithm for NO_2 vertical column retrieval from the ozone monitoring instrument, *Geoscience and Remote Sensing, IEEE Trans.*, *44*(5), 1245–1258, doi:10.1109/TGRS.2005.863715.
- Cazorla, M., W. H. Brune, X. Ren, and B. Lefer (2012), Direct measurement of ozone production rates in Houston in 2009 and comparison with two estimation methods, *Atmos. Chem. Phys.*, *12*(2), 1203–1212, doi:10.5194/acp-12-1203-2012.
- Chameides, W. L., et al. (1992), Ozone precursor relationships in the ambient atmosphere, *J. Geophys. Res.*, *97*(D5), 6037–6055, doi:10.1029/91JD03014.
- Choi, Y., Y. Wang, T. Zeng, R. V. Martin, T. P. Kurosu, and K. Chance (2005), Evidence of lightning NO_x and convective transport of pollutants in satellite observations over North America, *Geophys. Res. Lett.*, *32*, L02805, doi:10.1029/2004GL021436.
- Choi, Y., Y. Wang, Q. Yang, D. Cunnold, T. Zeng, C. Shim, M. Luo, A. Eldering, E. Bucselo, and J. Gleason (2008a), Spring to summer northward migration of high O_3 over the western North Atlantic, *Geophys. Res. Lett.*, *35*, L04818, doi:10.1029/2007GL032276.
- Choi, Y., Y. Wang, T. Zeng, D. Cunnold, E.-S. Yang, R. Martin, K. Chance, V. Thouret, and E. Edgerton (2008b), Springtime transitions of NO_2 , CO, and O_3 over North America: Model evaluation and analysis, *J. Geophys. Res.*, *113*, D20311, doi:10.1029/2007JD009632.
- de Arellano, J. V.-G., E. G. Patton, T. Karl, K. van den Dries, M. C. Barth, and J. J. Orlando (2011), The role of boundary layer dynamics on the diurnal evolution of isoprene and the hydroxyl radical over tropical forests, *J. Geophys. Res.*, *116*, D07304, doi:10.1029/2010JD014857.
- Eskes, H. J., and K. F. Boersma (2003), Averaging kernels for DOAS total-column satellite retrievals, *Atmos. Chem. Phys.*, *3*(5), 1285–1291, doi:10.5194/acp-3-1285-2003.
- Fiedler, V., et al. (2005), The contribution of sulphuric acid to atmospheric particle formation and growth: A comparison between boundary layers in Northern and Central Europe, *Atmos. Chem. Phys.*, *5*(7), 1773–1785, doi:10.5194/acp-5-1773-2005.
- Gilliam, R. C., and J. E. Pleim (2010), Performance assessment of new land surface and planetary boundary layer physics in the WRF-ARW, *J. Appl. Meteorol. Climatol.*, *49*, doi:10.1175/2009JAMC2126.1.
- Gray, B. A., Y. Wang, D. Gu, A. Bandy, L. Mauldin, A. Clarke, B. Alexander, and D. D. Davis (2011), Sources, transport, and sinks of SO_2 over the equatorial Pacific during the Pacific atmospheric sulfur experiment, *J. Atmos. Chem.*, *68*(1), 27–53, doi:10.1007/s10874-010-9177-7.
- Gu, D., Y. Wang, C. D. Smeltzer, and Z. Liu (2013), Reduction in NO_x emission trends over China: Regional and seasonal variations, *Environ. Sci. Technol.*, doi:10.1021/es401727e.
- Gu, D., Y. Wang, C. D. Smeltzer, and K. F. Boersma (2014), Anthropogenic emissions of NO_x over China: Reconciling the difference of inverse modeling results using GOME-2 and OMI measurements, *J. Geophys. Res. Atmos.*, *119*, 7732–7740, doi:10.1002/2014JD021644.
- Hains, J. C., et al. (2010), Testing and improving OMI DOMINO tropospheric NO_2 using observations from the DANDELIONS and INTEX-B validation campaigns, *J. Geophys. Res.*, *115*, D05301, doi:10.1029/2009JD012399.
- Heckel, A., S. W. Kim, G. J. Frost, A. Richter, M. Trainer, and J. P. Burrows (2011), Influence of low spatial resolution a priori data on tropospheric NO_2 satellite retrievals, *Atmos. Meas. Tech.*, *4*(9), 1805–1820, doi:10.5194/amt-4-1805-2011.
- Heffter, J. L. (1980), Transport layer depth calculations, in *Second Joint Conference on Applications of Air Pollution Meteorology*, pp. 787–791, Am. Meteorol. Soc., New Orleans, La.
- Hong, S.-Y., Y. Noh, and J. Dudhia (2006), A new vertical diffusion package with an explicit treatment of entrainment processes, *Mon. Weather Rev.*, *134*(9), 2318–2341, doi:10.1175/MWR3199.1.
- Hu, X.-M., J. W. Nielsen-Gammon, and F. Zhang (2010), Evaluation of three planetary boundary layer schemes in the WRF model, *J. Appl. Meteorol. Climatol.*, *49*(9), 1831–1844, doi:10.1175/2010jamc2432.1.
- Huijnen, V., et al. (2010), Comparison of OMI NO_2 tropospheric columns with an ensemble of global and European regional air quality models, *Atmos. Chem. Phys.*, *10*(7), 3273–3296.
- Janjić, Z. I. (1990), The step-mountain coordinate: Physical package, *Mon. Weather Rev.*, *118*(7), 1429–1443, doi:10.1175/1520-0493(1990)118<1429:TSMCPP>2.0.CO;2.
- Kanaya, Y., M. Fukuda, H. Akimoto, N. Takegawa, Y. Komazaki, Y. Yokouchi, M. Koike, and Y. Kondo (2008), Urban photochemistry in central Tokyo: 2. Rates and regimes of oxidant ($\text{O}_3 + \text{NO}_2$) production, *J. Geophys. Res.*, *113*, D06301, doi:10.1029/2007JD008671.
- Kleinman, L. I., P. H. Daum, Y. N. Lee, L. J. Nunnermacker, S. R. Springston, J. Weinstein-Lloyd, and J. Rudolph (2005), A comparative study of ozone production in five U.S. metropolitan areas, *J. Geophys. Res.*, *110*, D02301, doi:10.1029/2004JD005096.

- Knepp, T., et al. (2013), Estimating surface NO₂ and SO₂ mixing ratios from fast-response total column observations and potential application to geostationary missions, *J. Atmos. Chem.*, *72*(3-4), 261–286, doi:10.1007/s10874-013-9257-6.
- Lamsal, L. N., R. V. Martin, A. Padmanabhan, A. van Donkelaar, Q. Zhang, C. E. Sioris, K. Chance, T. P. Kurosu, and M. J. Newchurch (2011), Application of satellite observations for timely updates to global anthropogenic NO_x emission inventories, *Geophys. Res. Lett.*, *38*, L05810, doi:10.1029/2010GL046476.
- Lee-Taylor, J., S. Madronich, B. Aumont, A. Baker, M. Camredon, A. Hodzic, G. S. Tyndall, E. Apel, and R. A. Zaveri (2011), Explicit modeling of organic chemistry and secondary organic aerosol partitioning for Mexico City and its outflow plume, *Atmos. Chem. Phys.*, *11*(24), 13,219–13,241, doi:10.5194/acp-11-13219-2011.
- Leigh, R. J., G. K. Corlett, U. Frieß, and P. S. Monks (2007), Spatially resolved measurements of nitrogen dioxide in an urban environment using concurrent multi-axis differential optical absorption spectroscopy, *Atmos. Chem. Phys.*, *7*(18), 4751–4762, doi:10.5194/acp-7-4751-2007.
- Lin, J. T., R. V. Martin, K. F. Boersma, M. Sneep, P. Stammes, R. Spurr, P. Wang, M. Van Roozendaal, K. Clémer, and H. Irie (2014), Retrieving tropospheric nitrogen dioxide from the ozone monitoring instrument: Effects of aerosols, surface reflectance anisotropy, and vertical profile of nitrogen dioxide, *Atmos. Chem. Phys.*, *14*(3), 1441–1461.
- Lindinger, W., A. Hansel, and A. Jordan (1998), Proton-transfer-reaction mass spectrometry (PTR-MS): On-line monitoring of volatile organic compounds at pptv levels, *Chem. Soc. Rev.*, *27*(5), 347–354.
- Liu, S. C., et al. (1992), A study of the photochemistry and ozone budget during the Mauna Loa Observatory Photochemistry Experiment, *J. Geophys. Res.*, *97*(D10), 10,463–10,471, doi:10.1029/91JD02298.
- Liu, Z., et al. (2010), Evidence of reactive aromatics as a major source of peroxy acetyl nitrate over China, *Environ. Sci. Technol.*, *44*(18), 7017–7022.
- Liu, Z., et al. (2012a), Summertime photochemistry during CAREBeijing-2007: RO_x budgets and O₃ formation, *Atmos. Chem. Phys.*, *12*(16), 7737–7752, doi:10.5194/acp-12-7737-2012.
- Liu, Z., et al. (2012b), Exploring the missing source of glyoxal (CHOCHO) over China, *Geophys. Res. Lett.*, *39*, L10812, doi:10.1029/2012GL051645.
- Liu, Z., Y. Wang, F. Costabile, A. Amoroso, C. Zhao, L. G. Huey, R. Stickel, J. Liao, and T. Zhu (2014), Evidence of aerosols as a media for rapid daytime HONO production over China, *Environ. Sci. Technol.*, *48*(24), 14,386–14,391, doi:10.1021/es504163z.
- Martin, R. V., C. E. Sioris, K. Chance, T. B. Ryerson, T. H. Bertram, P. J. Wooldridge, R. C. Cohen, J. A. Neuman, A. Swanson, and F. M. Flocke (2006), Evaluation of space-based constraints on global nitrogen oxide emissions with regional aircraft measurements over and downwind of eastern North America, *J. Geophys. Res.*, *111*, D15308, doi:10.1029/2005JD006680.
- Mellor, G. L., and T. Yamada (1982), Development of a turbulence closure model for geophysical fluid problems, *Rev. Geophys.*, *20*(4), 851–875, doi:10.1029/RG020i004p00851.
- Ng, N. L., et al. (2007), Effect of NO_x level on secondary organic aerosol (SOA) formation from the photooxidation of terpenes, *Atmos. Chem. Phys.*, *7*(19), 5159–5174, doi:10.5194/acp-7-5159-2007.
- Petrìtoli, A., P. Bonasoni, G. Giovanelli, F. Ravegnani, I. Kostadinov, D. Bortoli, A. Weiss, D. Schaub, A. Richter, and F. Fortezza (2004), First comparison between ground-based and satellite-borne measurements of tropospheric nitrogen dioxide in the Po basin, *J. Geophys. Res.*, *109*, D15307, doi:10.1029/2004JD004547.
- Pleim, J. E. (2007), A combined local and nonlocal closure model for the atmospheric boundary layer. Part II: Application and evaluation in a mesoscale meteorological model, *J. Appl. Meteorol. Climatol.*, *46*(9), 1396–1409, doi:10.1175/JAM2534.1.
- Pleim, J. E. (2011), Comment on “simulation of surface ozone pollution in the Central Gulf Coast region using WRF/Chem model: Sensitivity to PBL and land surface physics”, *Adv. Meteorol.*, *2011*, 1–3, doi:10.1155/2011/464753.
- Ren, X. (2003), OH and HO₂ chemistry in the urban atmosphere of New York City, *Atmos. Environ.*, *37*, doi:10.1016/S1352-2310(03)00459-X.
- Ren, X., et al. (2013), Atmospheric oxidation chemistry and ozone production: Results from SHARP 2009 in Houston, Texas, *J. Geophys. Res.*, *118*, 5770–5780, doi:10.1002/jgrd.50342.
- Russell, A. R., A. E. Perring, L. C. Valin, E. J. Bucsela, E. C. Browne, P. J. Wooldridge, and R. C. Cohen (2011), A high spatial resolution retrieval of NO₂ column densities from OMI: Method and evaluation, *Atmos. Chem. Phys.*, *11*(16), 8543–8554, doi:10.5194/acp-11-8543-2011.
- Sachse, G. W., G. F. Hill, L. O. Wade, and M. G. Perry (1987), Fast response, high precision carbon monoxide sensor using a tunable diode laser absorption technique, *J. Geophys. Res.*, *92*, 2071–2081, doi:10.1029/JD092iD02p02071.
- Sander, S. P., et al. (2011), Chemical kinetics and photochemical data for use in atmospheric studies, Evaluation No.17, JPL Publ. 10-6, Rep., Jet Propul. Lab., Pasadena, Calif.
- Shin, H. H., and S.-Y. Hong (2011), Intercomparison of planetary boundary-layer parametrizations in the WRF model for a single day from CASES-99, *Boundary Layer Meteorol.*, *139*, doi:10.1007/s10546-010-9583-z.
- Shirley, T. R., et al. (2006), Atmospheric oxidation in the Mexico City Metropolitan Area (MCMA) during April 2003, *Atmos. Chem. Phys.*, *6*(9), 2753–2765, doi:10.5194/acp-6-2753-2006.
- Sillman, S. (2000), Ozone production efficiency and loss of NO_x in power plant plumes: Photochemical model and interpretation of measurements in Tennessee, *J. Geophys. Res.*, *105*(D7), 9189–9202, doi:10.1029/1999JD901014.
- Singh, H. B., et al. (2007), Reactive nitrogen distribution and partitioning in the North American troposphere and lowermost stratosphere, *J. Geophys. Res.*, *112*, D12S04, doi:10.1029/2006JD007664.
- Spicer, C. W. (1982), Nitrogen-oxide reactions in the urban plume of Boston, *Science*, *215*(4536), 1095–1097, doi:10.1126/science.215.4536.1095.
- Valks, P., G. Pinardi, A. Richter, J. C. Lambert, N. Hao, D. Loyola, M. Van Roozendaal, and S. Emmadi (2011), Operational total and tropospheric NO₂ column retrieval for GOME-2, *Atmos. Meas. Tech. Discuss.*, *4*(2), 1617–1676, doi:10.5194/amtd-4-1617-2011.
- Wang, Y. H., Y. Choi, T. Zeng, D. Davis, M. Buhr, L. G. Huey, and W. Neff (2007), Assessing the photochemical impact of snow NO_x emissions over Antarctica during ANTCTI 2003, *Atmos. Environ.*, *41*(19), 3944–3958.
- Weibring, P., D. Richter, J. G. Walega, L. Rippe, and A. Fried (2010), Difference frequency generation spectrometer for simultaneous multi-species detection, *Opt. Express*, *18*(26), 27,670–27,681, doi:10.1364/OE.18.027670.
- Xie, B., J. C. H. Fung, A. Chan, and A. Lau (2012), Evaluation of nonlocal and local planetary boundary layer schemes in the WRF model, *J. Geophys. Res.*, *117*, D12103, doi:10.1029/2011JD017080.
- Yang, Q., D. M. Cunnold, Y. Choi, Y. Wang, J. Nam, H.-J. Wang, L. Froidevaux, A. M. Thompson, and P. K. Bhartia (2010), A study of tropospheric ozone column enhancements over North America using satellite data and a global chemical transport model, *J. Geophys. Res.*, *115*, D08302, doi:10.1029/2009JD012616.
- Yerramilli, A., V. S. Challa, V. B. R. Dodla, H. P. Dasari, J. H. Young, C. Patrick, J. M. Baham, R. L. Hughes, M. G. Hardy, and S. J. Swanner (2010), Simulation of surface ozone pollution in the central Gulf coast region using WRF/Chem model: Sensitivity to PBL and land surface physics, *Adv. Meteorol.*, *2010*, 1–24, doi:10.1155/2010/319138.
- Zhang, Y., Y. Wang, B. A. Gray, D. Gu, L. Mauldin, C. Cantrell, and A. Bandy (2014), Surface and free tropospheric sources of methanesulfonic acid over the tropical Pacific Ocean, *Geophys. Res. Lett.*, *41*, 5239–5245, doi:10.1002/2014GL060934.

- Zhao, C., and Y. Wang (2009), Assimilated inversion of NO_x emissions over east Asia using OMI NO₂ column measurements, *Geophys. Res. Lett.*, *36*, L06805, doi:10.1029/2008GL037123.
- Zhao, C., Y. Wang, Y. Choi, and T. Zeng (2009a), Summertime impact of convective transport and lightning NO_x production over North America: Modeling dependence on meteorological simulations, *Atmos. Chem. Phys.*, *9*(13), 4315–4327, doi:10.5194/acp-9-4315-2009.
- Zhao, C., Y. Wang, and T. Zeng (2009b), East China plains: A “basin” of ozone pollution, *Environ. Sci. Technol.*, *43*(6), 1911–1915, doi:10.1021/es8027764.
- Zhao, C., Y. Wang, Q. Yang, R. Fu, D. Cunnold, and Y. Choi (2010), Impact of East Asian summer monsoon on the air quality over China: View from space, *J. Geophys. Res.*, *115*, D09301, doi:10.1029/2009JD012745.